Proc. Natl. Acad. Sci. USA
Vol. 93, pp. 12229–12234, October 1996
Biochemistry

Binding of the cellulose-binding domain of exoglucanase Cex from *Cellulomonas fimi* to insoluble microcrystalline cellulose is entropically driven

(titration microcalorimetry/binding thermodynamics/affinity purifications)

A. LOUISE CREAGH*, EDGAR ONG†, ERIC JERVIS*, DOUGLAS G. KILBURN†, AND CHARLES A. HAYNES*‡

Biotechnology Laboratory and Departments of *Chemical Engineering and †Microbiology and Immunology, University of British Columbia, Vancouver, BC, V6T 1Z3 Canada

Communicated by J. M. Prausnitz, University of California, Berkeley, CA, August 5, 1996 (received for review February 9, 1996)

ABSTRACT **Isothermal titration microcalorimetry is combined with solution-depletion isotherm data to analyze the thermodynamics of binding of the cellulose-binding domain (CBD) from the β-1,4-(exo)glucanase Cex of *Cellulomonas fimi* to insoluble bacterial microcrystalline cellulose. Analysis of isothermal titration microcalorimetry data against two putative binding models indicates that the bacterial microcrystalline cellulose surface presents two independent classes of binding sites, with the predominant high-affinity site being characterized by a Langmuir-type K_a of 6.3 (± 1.4) × 10^7 M^{-1} and the low-affinity site by a K_a of 1.1 (± 0.6) × 10^6 M^{-1}. CBD_{Cex} binding to either site is exothermic, but is mainly driven by a large positive change in entropy. This differs from protein binding to soluble carbohydrates, which is usually driven by a relatively large exothermic standard enthalpy change for binding. Differential heat capacity changes are large and negative, indicating that sorbent and protein dehydration effects make a dominant contribution to the driving force for binding.**

Many fungal and bacterial enzymes that hydrolyze insoluble carbohydrates have a modular structure and contain a discrete binding domain, which mediates binding to the polysaccharide (1, 2). The β-1,4-(exo)glucanase Cex, a major extracellular enzyme produced when the bacterium *Cellulomonas fimi* is grown on microcrystalline cellulose, is comprised of an N-terminal catalytic domain separated by a proline–threonine linker from a noncatalytic cellulose-binding domain CBD_{Cex} (3). CBD_{Cex} binds to many forms of insoluble cellulose, including amorphous, semi-crystalline, and crystalline, either as part of Cex or alone, when genetically or chemically separated from the catalytic domain and the proline–threonine linker (4, 5). Fusion proteins containing a CBD retain the biological activity of the fusion partner and bind strongly to cellulose, thereby providing a purification system that uses an inexpensive and readily available affinity matrix (6, 7).

CBDs have been identified in over 100 β-1,4-glucanases and can be grouped into nine structural families (I–IX) based on amino acid sequence homology (1). CBD_{Cex} belongs to family II, currently the largest family, with over 30 members (all of bacterial origin) including 7 found in *C. fimi* β-1,4-glycanases. All family II CBDs contain ≈100 amino acid residues and are stabilized by a disulfide bond between cysteines near each end (3). Highly conserved residues among family II members include four tryptophans (corresponding to W17, W38, W54, and W72 in CBD_{Cex}), two of which (corresponding to W17 and W72 in CBD_{Cex}) have been implicated in binding of a related family II member, CBD_{CenA} of endoglucanase A from *C. fimi*, through site-directed mutagenesis experiments (8).

The publication costs of this article were defrayed in part by page charge payment. This article must therefore be hereby marked "*advertisement*" in accordance with 18 U.S.C. §1734 solely to indicate this fact.

The solution structure of CBD_{Cex}, recently solved by multidimensional multinuclear NMR spectroscopy, shows that two of the conserved tryptophan residues (W54 and W72) are positioned at the surface, in fairly close proximity, and among a cluster of hydrophobic residues and hydrogen bond donors and acceptors, which together form a potential (relatively hydrophobic) binding ridge that terminates at a third fully exposed tryptophan, W17 (9). The driving force(s) and mechanism of CBD_{Cex} adsorption to insoluble cellulose are not known, but the conservation of the solvent-exposed linearly aligned tryptophan residues W17, W54, and W72 suggests that they participate in binding. Indirect support for this argument comes from evidence that tryptophan residues are directly involved in binding of soluble sugars to the maltodextrin-binding protein of *Escherichia coli* (10) and to other carbohydrate antigens (11–14). Here we describe the first microcalorimetric study of binding of a carbohydrate-binding protein to an insoluble oligosaccharide suspension with the aim of determining the thermodynamic driving force(s) for binding of CBD_{Cex} to bacterial microcrystalline cellulose (BMCC), as well as the possibility of gaining some understanding of differences in driving forces for binding of soluble and insoluble polysaccharides.

MATERIALS AND METHODS

Protein Production, Purification, and Characterization. The gene fragment encoding the CBD of the exoglucanase Cex from *C. fimi* was subcloned into the pTZEO7 vector and expressed in *E. coli* strain JM101. Production of CBD_{Cex} followed the protocol of Ong *et al.* (15) and yielded ≈60 $mg \cdot liter^{-1}$ (culture supernatant) of soluble protein in a 20-liter fermentor (Chemap, Mannedorf, Switzerland) operated at 37°C with a 10-liter working volume controlling pO_2 at 50 mmHg (pH 7.0).

Initial purification of CBD_{Cex} from culture supernatant followed the affinity precipitation method of Ong *et al.* (15). Contaminant oligosaccharide was removed by size exclusion chromatography on a Superose-12 column (Pharmacia). One-half milliliter aliquots of CBD_{Cex} (10 $mg \cdot ml^{-1}$) in 100 mM potassium phosphate buffer (pH 7.0) containing 150 mM NaCl were passed through the column (0.3–0.5 $ml \cdot min^{-1}$), previously equilibrated with the same buffer. Protein fractions (A_{280nm}) devoid of carbohydrate (A_{490nm}) were pooled, concentrated, and dialyzed against distilled water or 50 mM potassium phosphate buffer (pH 7.0).

Abbreviations: CBD, cellulose-binding domain; BMCC, bacterial microcrystalline cellulose; ITC, isothermal titration calorimetry; FITC, fluorescein isothiocyanate.

‡To whom reprint requests should be addressed at: Biotechnology Laboratory and Department of Chemical Engineering, University of British Columbia, 237 Wesbrook Building, 6174 University Boulevard, Vancouver, BC, V6T 1Z3 Canada.

Sorbents and Reagents. BMCC was prepared from cultures of *Acetobacter xylinum* (ATCC 23769) grown on peptone/yeast extract/glucose medium according to the method of Gilkes *et al.* (16). All water was purified through a Barnsted Nanopure II water-purification system.

Binding Isotherm Measurements. All adsorption–isotherm measurements were carried out at 30°C (± 0.3°C) in 1.5-ml Eppendorf tubes containing 1–300 μM of CBD_{Cex} mixed with 1 mg of BMCC in 50 mM phosphate buffer [pH 7 (± 0.1)], to a final aqueous volume of 1.0 ml. Control tubes contained no BMCC. Each solution was vortexed for ≈5 sec and then rotated end-over-end for 16 hr to allow the adsorption system to equilibrate. The samples were then centrifuged at 30°C and 10,000 rpm for 10 min to remove the protein-covered BMCC; the clear supernatant was collected and passed through a 0.2-μm Acrodisc filter (Gelman) on which no protein adsorption could be detected. The depletion method, based on the A_{280nm} reading of the supernatant, was then used to calculate the amount of CBD_{Cex} adsorbed to the BMCC. Desorption isotherm data were taken by serial dilution of an equilibrium adsorption solution prepared in the manner described above. Each measurement was done in triplicate. CBD_{Cex} function is not affected by vortexing, as indicated by identical binding isotherms for vortexed and unvortexed controls.

Titration Microcalorimetry. All isothermal titration calorimetry (ITC) experiments were carried out at pH 7 in either an LKB 2277 Thermal Activity Monitor or a Calorimetry Sciences (Provo, UT) 4200 ITC. Three sets of ITC experiments for CBD_{Cex} binding to a fixed weight of BMCC were performed: (*i*) variable-composition binding enthalpy $\Delta H°$ measurements to determine binding energetics, (*ii*) variable-temperature $\Delta H°$ measurements to determine differential heat capacities ΔC_p of binding, and (*iii*) variable ionic-strength $\Delta H°$ measurements to assess the contribution of electrostatic forces to the overall driving force for binding. The reference was 50 mM potassium phosphate buffer (pH 7) for all measurements. All calorimetric data are reported per mole of CBD_{Cex}.

All titrant and titrate solutions were thoroughly degassed under vacuum prior to loading in the ITC. Between 1 and 1.5 ml of titrate solution containing 50 mM phosphate buffer (pH 7.0), 0.01% sodium azide, and 0.1 mg of BMCC were loaded into the 2-ml ITC sample cell and allowed to equilibrate to the set-point temperature (either 25°C, 30°C, or 35°C) for 2–3 hr under continuous mixing at 300 rpm. These mixing conditions were sufficient to create a homogeneous suspension of the insoluble BMCC fibers such that mass transfer did not limit the binding event. Binding studies at different mixing speeds indicated that binding was mass-transfer limited at speeds below ≈200 rpm, but remained constant and thermodynamically limited at speeds above 200 rpm. Twenty, 12-μl titrant samples containing between 0.1 and 0.3 mM CBD_{Cex}/0.01% sodium azide in 50 mM phosphate buffer were injected into the sample cell at 10-min intervals from a 250-μl Hamilton syringe. The nonlinear least-squares algorithm used to analyze the raw titration data follows that developed by Wiseman *et al.* (17) yielding K_a and $\Delta H°$.

Differential heat capacities are determined by applying the finite differential form of the fundamental thermodynamic definition for $\Delta C_p° = (\partial H/\partial T)_p \approx (\Delta H°/\Delta T)_p$ to measured binding enthalpies at 25°C, 30°C, and 35°C and otherwise constant conditions.

Confocal Microscopy. Fluorescein isothiocyanate (FITC)-labeled CBD_{Cex} was prepared by adding 0.15 mg FITC per mg of protein and 1 μl NaOH per ml of sample solution containing 1.0 mg/ml CBD_{Cex} in NaN_3-free PBS buffer (18). The reaction mixture was then gently mixed at ambient temperature in the dark for 5 hr. The labeled protein was passed through a 5-ml Sephadex G50 gel filtration column with 50 mM phosphate buffer (pH 7.0 and 0.02% NaN_3) mobile phase at 1 ml/min to separate unbound FITC from labeled protein. Absorbance readings at 280 nm and 405 nm were measured on the pooled fractions to determine final protein concentration and the FITC:CBD_{Cex} labeling ratio, respectively, the latter of which was determined to be 1.65 FITC residues bound per protein molecule. All labeled protein was stored at 4°C until use.

Binding of FITC-labeled CBD_{Cex} on BMCC was measured as described above for 0.5-ml samples containing 0.15 mg BMCC and either 1.0 μM of protein, a subsaturating binding level where $[B] = 0.03[B]^{pl}$ ($[B]^{pl}$ is the plateau binding level) or 30 μM of protein where $[B] = [B]^{pl}$. The samples were equilibrated for 30 min, then centrifuged for 10 min at 10,000 rpm and the free solution removed by pipette. Residual unbound protein was removed by washing the BMCC pellet twice with 1.5 ml of PBS. A sample of the labeled pellet was then transferred to a microscope slide and covered with a No. 1 glass coverslip sealed with DPX mountant around the edges to prevent evaporation during imaging. The mass balance relating bound and unbound protein was verified by direct fluorescence imaging of the solution and sorbent.

A Bio-Rad MRC600 confocal microscope was used to image the labeled BMCC fibrils. A 60× Nikon objective was used with a numerical aperture of 1.4; the photomultiplier gain and black current level were set to 7 and 4.7, respectively; the confocal aperture, which regulates the axial depth of the imaged fibers, was set to 10 (19). Images were collected using Kalman filtering over three successive scans to reduce noise in the final image. No other image filtering or contrast enhancement manipulations were performed.

RESULTS

Binding Model and Stoichiometry. Two putative models for equilibrium binding were compared by combining each with the nonlinear analysis described above to regress binding constants and stoichiometries for binding of CBD_{Cex} to an insoluble (fully suspended) BMCC matrix of known dry weight but unknown surface area. In each model, [F] is the equilibrium concentration of unbound protein (M), [B] is the bound protein concentration (mol/g BMCC), and [N] is the equilibrium concentration of available binding sites on the BMCC substrate (mol/g BMCC) so that

$$K_a\,(M^{-1}) = \frac{[B]}{[N][F]}. \qquad [1]$$

Model I, an adaptation of the Langmuir equilibrium binding model (16), follows from the RMDw structure of CBD_{Cex} (9), which indicates that the projected area of a bound CBD_{Cex} molecule on BMCC is ≈29 (± 2) times the side-on surface area of the repeating cellobiose lattice unit when the proposed tryptophan-rich binding ridge of CBD_{Cex} is positioned toward the sorbent. Thus, CBD_{Cex} blocks a number of lattice sites in addition to the one(s) to which it is specifically bound. Model I accounts for this blocking effect by treating the sorbent as an array of overlapping identical binding sites such that

$$[B] = \frac{[N]_0 K_a[F]}{1 + \mathfrak{a}K_a[F]}, \qquad [2]$$

where $\mathfrak{a}$ is the number of (cellobiose) lattice units occupied by a single CBD_{Cex} molecule and $[N]_o$ is the total concentration (mol/g BMCC) of lattice units on the BMCC sorbent. Eq. **2** is strictly valid only at conditions where $\mathfrak{a}[B]/[N]_o \ll 1$ and, thus, can only be applied to the regression of binding data at low protein concentrations (i.e., the initial slope of the binding isotherm). Under these limiting conditions, the binding and saturation parameters in Model I are related to those of conventional Langmuir theory (K_{aL} and $[N]_{oL}$, respectively) by $K_a = K_{aL}/\mathfrak{a}$ and $[N]_o = \mathfrak{a}[N]_{oL}$. Gilkes *et al.* (16) estimated $[N]_o$ to be 101 μmol cellobiose units/g BMCC based on crystallo-

graphic data and evidence that *Trichoderma reesei* and *C. fimi* cellulases preferentially bind to the 110 face of algal cellulose crystals. If so, regression of Eq. **2** to adsorption isotherm data for CBD_{Cex} on BMCC should yield a value for $[N]_{oL}$ close to 3.5.

Model II assumes heterogeneity in a Langmuir-type sorbent surface such that two independent classes of binding sites are present:

$$[B] = \frac{[N_I]_{oL}K_{aL}^{I}[F]}{1 + K_{aL}^{I}[F]} + \frac{[N_{II}]_{oL}K_{aL}^{II}[F]}{1 + K_{aL}^{II}[F]}, \qquad [3]$$

where $[N_I]_{oL}$ is the total concentration of class I binding sites characterized by a binding constant K_{aL}^{I} and $[N_{II}]_{oL}$ is the total concentration of class II binding sites characterized by a binding constant K_{aL}^{II}.

Fig. 1 shows the ascending binding isotherm for CBD_{Cex} on BMCC in 50 mM phosphate buffer at pH 7.0 and 30°C as determined from ITC data. Binding isotherm data for the same system determined by the conventional depletion method are also shown in Fig. 1 and are in close agreement with the ITC data. Comparison of differential scanning calorimetry thermograms for free and bound CBD_{Cex} indicates that the native solution structure of CBD_{Cex} is not altered during the binding process. The near-infinite initial slope of the isotherm indicates that CBD_{Cex} has a high affinity for the BMCC surface. Both isotherms fold over at a surface coverage of 4 (± 0.3) μmol CBD_{Cex}/g BMCC, which equates to a surface concentration of ≈45 mg CBD_{Cex}/g BMCC. However, the bound protein concentration [B] never reaches a clear plateau, but instead slowly rises with increasing free protein concentration [F].

Results from least-squares regressions of the two putative binding models for CBD_{Cex} on BMCC are shown in Table 1. Regression of $[N]_o$ and K_a in Model I, with the aspect ratio **a** set at 29 in accordance with the NMR data, was restricted to low concentrations (i.e., [F] < 0.2 μM). This yields an $[N]_{oL}$ value of 3.43 (± 0.04) μmol/g BMCC and, thus, an $[N]_o$ value of 99 (± 4) μmol/g BMCC, which is consistent with that estimated by Gilkes *et al.* (16).

Only two ($[N_{II}]_{oL}$ and K_{aL}^{II}) of the four parameters in the two-site model were adjusted by nonlinear least-squares regression to fit Eq. 3 to the entire binding curve. The remaining two parameters, $[N_I]_{oL}$ and K_{aL}^{I}, were fixed at the values (3.43 μmol/g BMCC and 6.3×10^7 M^{-1}, respectively) determined by fitting the conventional Langmuir model to the low-concentration region. Restricting the number of adjustable parameters in model II can be justified in two ways: (*i*) the initial slopes of binding isotherms for multi-site binding systems are dominated by that subset of sites that has the highest affinity for the sorbate molecule (20) and (*ii*) a fair comparison of the two putative models must be based on an equal number of adjustable parameters. However, application of the probability statistical analysis of Franco *et al.* (21) to the two models shows that adjustment of two parameters in the four-parameter two-site model has a slightly higher (5.2%) intrinsic probability of a successful fit than the two-parameter model under consideration. This intrinsic advantage of the two-site model was eliminated prior to comparing the two putative models by weighting the calculated probability that model *i*, out of *m* different proposed binding models, is correct against the intrinsic probability that it will yield the best fit based on model structure alone (13, 21). For each putative model, Table 1 shows the calculated probability $P(i)$ that the model provides the correct description of the binding interaction(s) based on regression of the entire set of ITC binding isotherm data shown in Fig. 1. The two-site model has a significantly higher probability of being correct.

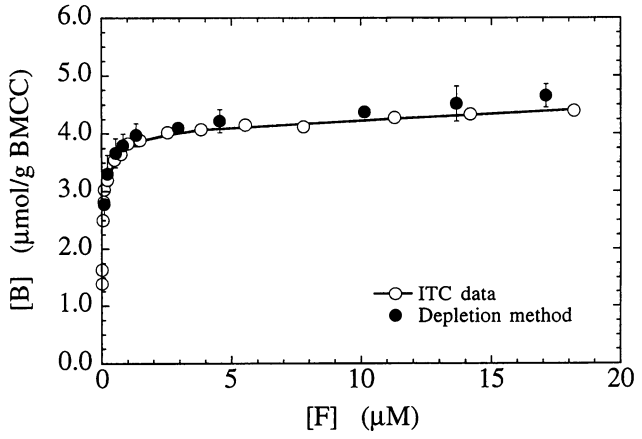

FIG. 1. Binding isotherm at 30°C for CBD_{Cex} on BMCC in 50 mM phosphate buffer at pH 7.0 measured both by the conventional solution depletion method and ITC.

Both models give a binding constant for the high-affinity class of binding sites of $K_{aL} = \mathbf{a}K_a = K_{aL}^{I} = 6.3 \times 10^7$ (± 1.4) M^{-1}, indicating that CBD_{Cex} is tightly bound. Results from the two-site model suggest that approximately 79% of all available binding sites on the BMCC surface are of the high-affinity type, whereas a low-affinity binding site characterized by a binding constant $K_{aL}^{II} = 1.1 \times 10^6$ M^{-1} accounts for ≈21% of the binding surface.

Fig. 2 compares confocal microscope images of the BMCC surface after adsorption of a submonolayer ($[B] = 0.03[B]^{pl}$) and monolayer of FITC-labeled CBD_{Cex} in 50 mM phosphate buffer at pH 7 and 30°C. Adsorption isotherms for CBD_{Cex} and FITC-CBD_{Cex} on BMCC show no dependence on the ratio of labeled to unlabeled protein, indicating that the FITC label does not interfere with binding. At low surface coverages (Fig. 2*A*), adsorbed CBD_{Cex} is evenly distributed throughout the fiber sample as evidenced by the uniform fluorescence intensity from the imaged fibers. In constrast, the image of the saturated surface (Fig. 2*B*) shows a small but significant amount of binding heterogeneity such that several small, very bright regions are apparent. The absence of brightness heterogeneities at low surface coverage suggests that the bright regions are not indicative of a higher affinity, but rather of an area of lower affinity but relatively high specific surface area. These low-affinity pockets of increased specific surface could be due to a number of effects, including fiber imperfections during biosynthesis leading to (semi)amorphous microstructures or to physical damage of the fibrils during their preparation from the BMCC pellicles.

Binding Thermodynamics from Titration Microcalorimetry. Fig. 3 shows the cumulative calorimetric heat for binding of CBD_{Cex} to BMCC in 50 mM phosphate buffer at pH 7.0 and 30°C. Binding is exothermic, reaching a saturation binding heat of 5.6 ± 0.3 kJ/mol. Fig. 3 also shows the best fit of the two-site model to the integral calorimetric heat assuming K_{aL}^{I} and K_{aL}^{II} are equal to 6.3×10^7 M^{-1} and 1.1×10^6 M^{-1}, respectively, as regressed from the binding isotherm data.

Table 2 reports binding thermodynamics results for each putative model fit to both integral and differential calorimetric heat data. For the single binding-class model I, the saturation calorimetric heat of −5.6 kJ/mol shown in Fig. 3 is equivalent to the standard enthalpy change $\Delta H°$ for the binding reaction. In the case of the two-site model, $\Delta H°$ is the sum of the standard enthalpy changes for binding to the high-affinity ($\Delta H_I°$) and low-affinity ($\Delta H_{II}°$) sites. Regression of the two-site model to both the integral and differential calorimetric heat data gives $\Delta H_I°$ and $\Delta H_{II}°$ values of −4.8 (± 0.3) kJ/mol and −0.8 (± 0.3) kJ/mol. Thus, irrespective of the binding model, the regressed standard enthalpy of binding for the high-affinity binding site is relatively small and favorable (i.e., exothermic). Entropy strongly favors binding, accounting for

Table 1. Regressed binding parameters from least-squares fitting of each putative model to the integral isothermal microcalorimetry data shown in Fig. 1 and the calculated probability $P(i)$ that each model i provides the most appropriate description of the binding reaction(s)

Putative model	$[N_I]$ (μmol/g BMCC)*	K_aI (M^{-1})†	$[N_{II}]_{oL}$ (μmol/g BMCC)	K_{aL}^{II} (M^{-1})	$P(i)$
I	3.43 (± 0.04)	6.3 (± 1.4) × 10^7	—	—	<0.01
II	3.43	6.3 × 10^7	0.9 (± 0.05)	1.1 (± 0.6) × 10^6	0.99

T = 30°C, pH 7.1, and the aspect ratio a set at 29.
*$[N_I] \equiv [N]_{oL} = [N]_o/a = [N_I]_{oL}$.
†$K_a^I \equiv K_{aL} = aK_a = K_{aL}^I$.

≈85% of the binding energy ΔG°. Binding to the low-affinity class of sites on BMCC is also entropically driven, with $\Delta H_{II}°$ making almost no contribution to the overall driving force for adsorption (ΔG°).

In contrast, ΔH° makes the dominant contribution to ΔG° in almost all of the soluble oligosaccharide binding systems investigated by titration microcalorimetry (22, 23). The largely entropically driven binding of CBD_{Cex} to microcrystalline cellulose therefore points to a difference in the nature of the binding mechanisms for soluble and insoluble (crystalline) polysaccharides.

Electrostatic Contributions to Binding. CBD_{Cex} has only a small number of residues that could protonate or deprotonate during binding to crystalline cellulose. Titratable groups on the surface of CBD_{Cex} include only the α-amino group at the N terminus, Lys-28, Asp-36, Arg-68, and His-90, none of which are located within the proposed cellulose binding ridge defined by tryptophan residues 17, 54, and 72. Below ≈pH 12, where the 2-hydroxyl is fully protonated, cellulose is a neutral polymer. This lack of fixed charge on the sorbent and protein surfaces suggests that electrostatics do not drive adsorption of CBD_{Cex} to BMCC.

Fig. 3 compares the cumulative calorimetric heat for binding of CBD_{Cex} to BMCC in 50 mM phosphate buffer at pH 7 and 30°C with that for binding in 5 mM phosphate buffer at otherwise identical conditions. Within experimental error, the two calorimetric binding isotherms are indistinguishable, both reaching a saturation binding heat of 5.6 ± 0.3 kJ/mol at a free protein concentration of ≈3 μM. This insensitivity to ionic strength indicates that charge redistribution effects do not make a dominant contribution to the driving force for adsorption. Additional data supporting this argument comes from Ong *et al.* (15), who found no pH dependence to the relative binding affinity of CBD_{Cex} for BMCC.

Protein and Sorbent Dehydration Effects. The differential heat capacity $\Delta C_p°$ for binding of CBD_{Cex} on BMCC at pH 7 (50 mM phosphate buffer) over the temperature range 25°C to 35°C is large and negative at all surface coverages. $\Delta C_p°$ reaches a minimum value of −2.46 kJ/mol K at $\Gamma = 0.7[B]^{pl}$ and increases to −1.53 kJ/mol K at monolayer coverage. Tanford (24), Dill (25), and others (26, 27) have argued that a negative $\Delta C_p°$ in aqueous mixing systems indicates a process for which dehydration effects make a dominant contribution. This suggests then that CBD_{Cex} and sorbent dehydration provide a major contribution to overall driving force for binding of CBD_{Cex} to BMCC. A second indication that the binding process is dominated by dehydration effects is provided by the large positive entropy change ΔS°, measured by ITC, due to the increased rotational and translational degrees of freedom of the water molecules released from the sorbent and protein surfaces during adsorption.

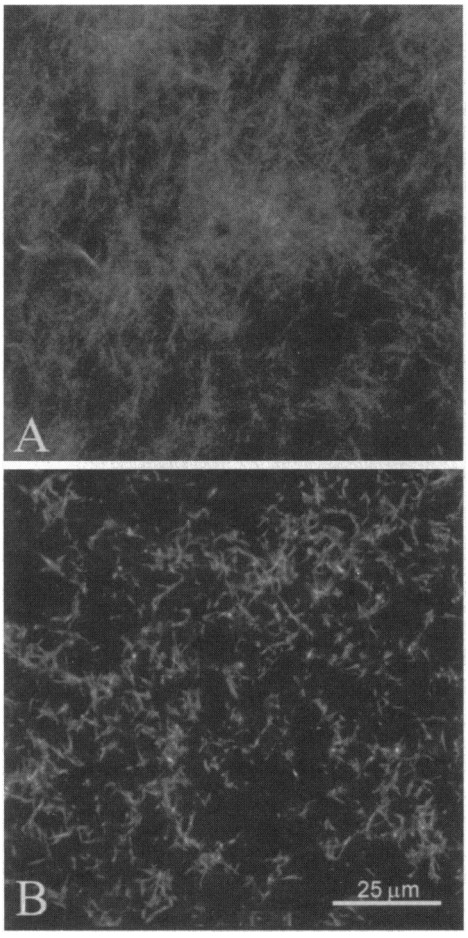

FIG. 2. Confocal microscope images of FITC-labeled CBD_{Cex} bound to BMCC in 50 mM phosphate buffer at pH 7.0 and 30°C. (*A*) Subsaturating binding level containing 1 μM protein such that $[B] = 0.03[B]^{pl}$. (*B*) Saturating binding level ($[B] = [B]^{pl}$) containing 30 μM protein.

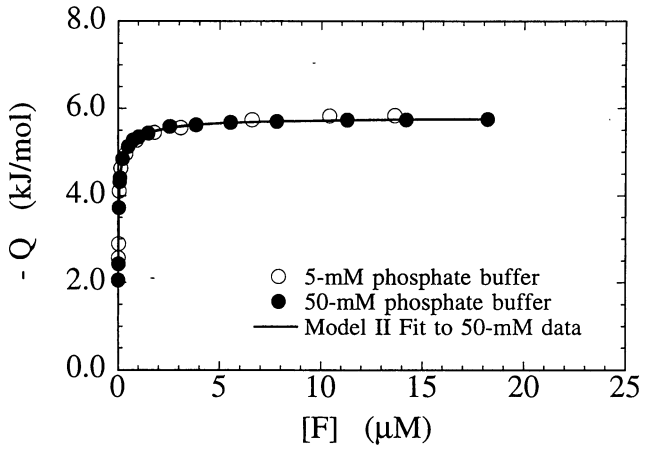

FIG. 3. Cumulative calorimetric heat curves for binding of CBD_{Cex} to BMCC in 50 mM and 5 mM phosphate buffer at pH 7.0 and 30°C. Solid curve is the best fit of the two-site model to the integral calorimetric heat.

Table 2. Binding thermodynamics results for each putative model fit to both integral (Int) and differential (Dif) calorimetric heat data

	$\Delta G°_I$ (kJ/mol)*		$\Delta H°_I$ (kJ/mol)		$T\Delta S°_I$ (kJ/mol)		$\Delta G°_{II}$ (kJ/mol)		$\Delta H°_{II}$ (kJ/mol)		$T\Delta S°_{II}$ (kJ/mol)	
Model	Dif	Int	Dif	Int	Dif	Int	Dif	Int	Dif	Int	Dif	Int
I	−36.4 (± 0.7)	−36.8 (± 0.5)	−5.8 (± 0.5)	−5.6 (± 0.3)	30.6 (± 1.2)	31.2 (± 0.8)	—	—	—	—	—	—
II	−44.1 (± 0.8)	−45.2 (± 0.6)	−4.9 (± 0.5)	−4.8 (± 0.3)	39.2 (± 1.3)	40.4 (± 0.9)	−34.5 (± 1.1)	−35.0 (± 0.9)	−0.9 (± 0.4)	−0.8 (± 0.3)	33.6 (± 1.5)	34.2 (± 1.2)

*For model I, $\Delta G° = -RT \ln K_a$, and for model II, $\Delta G° = -RT \ln K_{aL}^I$.

DISCUSSION

Entropic Effects Drive Binding. A central difference between soluble polysaccharide binding systems and binding of CBD_{Cex} to insoluble microcrystalline cellulose is the structure and conformational freedom of the ligand. Tight binding of soluble oligosaccharides requires a loss in conformational entropy for that portion of the polymer chain in direct contact with the protein binding site, which compensates the entropy gain associated with dehydration of the protein–ligand contact surface. In contrast, the conformation of each cellulose chain on the fiber surface of BMCC is essentially fixed and, thus, the chain is unlikely to undergo a loss in conformational entropy upon binding to CBD_{Cex}. This, combined with the negative ΔC_p values that indicate a significant dehydration effect, provides an explanation of the large favorable $\Delta S°$ observed for CBD_{Cex} adsorption to BMCC and points toward a fundamental difference between binding of soluble and insoluble polysaccharides.

Binding Enthalpy. As with most sugar binding systems characterized to date by calorimetry, binding of CBD_{Cex} to BMCC is exothermic. However, the magnitude of the cumulative enthalpic driving force for binding ($\Delta H° = -5.6$ kJ/mol) is smaller than typical values for binding of soluble sugars which range from ≈ -15 to -100 kJ/mol (14, 22, 23). In soluble random-coil polysaccharide binding systems, the formation of multiple contacts and optimal interatomic distances is facilitated by the relatively high conformational freedom of the ligand. In contrast, the rigidity of cellulose chains on the BMCC surface minimizes the ability of the ligand to mold itself to the CBD_{Cex} binding surface, resulting in a comparatively small $\Delta H°$.

A proposed binding complex consistent with all of these thermodynamic data is one where a number of the residues along the tryptophan-rich binding ridge of CBD_{Cex} make enthalpically weak but sufficient contacts with the largely inflexible BMCC surface to dehydrate both the binding ridge and the underlying sorbent. Specificity of binding is likely determined by the energetic driving force for formation of intermolecular hydrogen bonds between dehydrated electron donors and acceptors on the contacting sorbent and protein surfaces. Formation of an (energetic) optimum number of hydrogen bonds may be facilitated by a disruption of fiber surface during binding, which exfoliates surface cellulose chains and their associated hydroxyl residues.

BMCC Appears to Offer Multiple Classes of Binding Sites to CBD_{Cex}. The successful fit of the two-state binding model combined with the confocal microscope images, which show heterogeneities in surface fluorescence intensities at high FITC-labeled CBD_{Cex} loads, indicate that BMCC offers two (significant) independent classes of binding sites to CBD_{Cex}.

Confocal microscope images of sequentially increasing surface concentration indicate that the degree of dispersion of the BMCC fibrils is dependent upon the concentration of bound CBD_{Cex}. At low concentrations of bound protein, the fibrils are flocculated into relatively large aggregates. As the surface concentration of CBD_{Cex} increases, the fibrils tend to disperse. The mechanism for this deflocculation is unknown, but the possibility that the process leads to an increase in the total number of binding sites on the BMCC surface with increasing protein concentration must be considered. Since the micromole of CBD_{Cex} adsorbed at a given total protein concentration is directly determined and therefore fixed by the depletion method, an increase in BMCC surface area per gram must result in a relative decrease in [B] compared with the value predicted by Langmuir theory.

Nevertheless, both sorbent deflocculation and overlapping binding-site effect may influence the binding constants. As a result, although a second low-affinity class of binding site is present on the BMCC surface, the magnitude of the associated binding constant should be viewed as qualitative rather than quantitative.

We gratefully acknowledge the help of Dr. Peter Tomme, who supplied some of the protein used in this work, and Drs. Neil Gilkes and Tony Warren. This work was funded by the Natural Science and Engineering Research Council of Canada and the Protein Engineering Network of Centres of Excellence.

1. Tomme, P., Warren, R. A. J. & Gilkes, N. (1995) *Adv. Microb. Physiol.* **37,** 1–81.
2. Svensson, B., Jespersen, H., Sierks, M. R. & MacGregor, E. A. (1989) *Biochem. J.* **264,** 309–311.
3. Gilkes, N. R., Henrissat, B., Kilburn, D. G., Miller, R. C., Jr., & Warren, R. A. J. (1991) *Microbiol. Rev.* **55,** 303–315.
4. Gilkes, N. R., Warren, R. A. J., Miller, R. C., Jr., & Kilburn, D. G. (1988) *J. Biol. Chem.* **263,** 10401–10407.
5. Greenwood, J. M., Gilkes, N. R., Kilburn, D. G., Miller, R. C., Jr., & Warren, R. A. J. (1989) *FEBS Lett.* **244,** 127–131.
6. Ong, E., Gilkes, N. R., Miller, R. C., Jr., Warren, R. A. J. & Kilburn, D. G. (1991) *Enzyme Microb. Technol.* **13,** 59–65.
7. Greenwood, J. M., Ong, E., Gilkes, N. R., Warren, R. A. J., Miller, R. C., Jr., & Kilburn, D. G. (1992) *Protein Eng.* **5,** 361–365.
8. Din, N., Forsythe, I. J., Burtnik, L. D., Gilkes, N. R., Miller, R. C., Jr., Warren, R. A. J. & Kilburn, D. G. (1994) *Mol. Microbiol.* **11,** 747–755.
9. Xu, G. Y., Ong, E., Gilkes, N. R., Kilburn, D. G., Muhandiram, D. R., Brandeis, M., Carver, J. P., Kay, L. E. & Harvey, T. S. (1995) *Biochemistry* **34,** 6993–7009.
10. Spurlino, J. C., Rodseth, L. E. & Quiocho, F. A. (1992) *J. Mol. Biol.* **226,** 15–22.
11. Vyas, N. K. (1991) *Curr. Opin. Struct. Biol.* **1,** 732–740.
12. Quiocho, F. A. (1989) *Pure Appl. Chem.* **61,** 1293–1306.
13. Sigurskjold, B. W., Svensson, B., Williamson, G. & Driguez, H. (1994) *Eur. J. Biochem.* **225,** 133–141.
14. Bundle, D. R., Eichler, E., Gidney, A. J., Meldel, M. A. J., Ragauskas, A., Sigurskjold, B. W., Sinnott, B., Watson, D. C., Yaguchi, M. & Young, N. M. (1994) *Biochemistry* **33,** 5172–5182.
15. Ong, E., Gilkes, N. R., Miller, R. C., Jr., Warren, R. A. J. & Kilburn, D. G. (1993) *Biotechnol. Bioeng.* **42,** 401–409.
16. Gilkes, N. R., Jervis, E., Henrissat, B., Tekant, B., Miller, R. C., Jr., Warren, R. A. J. & Kilburn, D. G. (1992) *J. Biol. Chem.* **267,** 6743–6749.
17. Wiseman, T., Williston, S., Brandts, J. F. & Lin, L.-N. (1989) *Anal. Biochem.* **17,** 131–137.
18. Brinkley, M. (1993) in *Perspectives in Bioconjugate Chemistry*, ed. Meares, C. F. (ACS, Washington, DC), pp. 59–70.
19. Mailof, L. & Forsgren, P. O. (1993) *Methods Cell Biol.* **38,** 79–95.
20. Everett, D. H. (1954) *Trans. Faraday Soc.* **50,** 1077–1096.
21. Franco, R., Gavaldà, M. T. & Canela, E. I. (1986) *Biochem. J.* **238,** 855–862.
22. Carver, J. P., Michnick, S. W., Imberty, A. & Cumming, D. A. (1989) *CIBA Found. Symp.* **145,** 6–26.

23. Goto, M., Tanigawa, K., Kanlayakrit, W. & Hayashida, S. (1994) *Biosci. Biotechnol. Biochem.* **58,** 49–54.
24. Tanford, C. (1973) *The Hydrophobic Effect* (Wiley–Interscience, New York).
25. Dill, K. (1990) *Biochemistry* **29,** 7133–7155.
26. Brandts, J. F., Jackson, W. M. & Ting, T. Y.-C. (1974) *Biochemistry* **13,** 3595–3600.
27. Wishnia, A. (1969) *Biochemistry* **8,** 5064–5070.